AIP Publishing

This manuscript was accepted by J. Appl. Phys. Click here to see the version of record.

In situ Imaging of the Soldering Reactions in Nanoscale Cu/Sn/Cu and Sn/Cu/Sn Diffusion Couples

Qiyue Yin[1], Fan Gao[2], Zhiyong Gu[2], Jirui Wang[2], Eric A. Stach[3], Guangwen Zhou[1*]

[1]Department of Mechanical Engineering & Materials Science and Engineering Program, State University of New York at Binghamton, NY 13902, USA

[2]Department of Chemical Engineering, University of Massachusetts Lowell, Lowell, MA 01854, USA

[3]Center for Functional Nanomaterials, Brookhaven National Laboratory, Upton, NY 11973, USA

Abstract

The soldering reactions of three-segmented Sn/Cu/Sn and Cu/Sn/Cu diffusion couples are monitored by in-situ transmission electron microscopy to reveal the metallurgical reaction mechanism and the associated phase transformation pathway. For Sn/Cu/Sn diffusion couples, there is no ε-Cu_3Sn formation due to the relatively insufficient Cu as compared to Sn. Kirkendall voids form initially in the Cu segment and then disappear due to the volume expansion associates with the continued IMC formation as the reaction progresses. The incoming Sn atoms react with Cu to form η-Cu_6Sn_5, and the continuous reaction then transforms the entire nanowire to η-Cu_6Sn_5 grains with remaining Sn. With continued heating slightly above the melting point of Sn, Sn-rich liquid phase forms between η-Cu_6Sn_5 grains. By contrast, the reaction in the Cu/Sn/Cu diffusion couples results in the intermetallic phases of both Cu_3Sn and Cu_6Sn_5 and the development of Cu_6Sn_5 bulges on Cu_3Sn grains. Kirkendall voids form in the two Cu segments, which grow and eventually break the nanowire into multiple segments.

*To whom correspondence should be addressed. Email: gzhou@binghamton.edu

ACCEPTED MANUSCRIPT

AIP Publishing

This manuscript was accepted by J. Appl. Phys. Click here to see the version of record.

1. Introduction

In the trend towards the greater integration, higher performance and further miniaturization of electronic devices there is an increasing need to develop and investigate interconnection materials on the sub-micrometer or nanometer scale. [1] Solders are extensively used in a wide range of electronic systems to form reliable joints between electronic components. [2] Extending the use of conventional solders to nanoscale is promising. Nanowires are one of the most studied one-dimensional (1D) nanostructures, as they can function as basic electronic circuit elements [3-5] or be assembled and integrated into 1D, 2D, or 3D functional structures. As a result, they have great potential in applications such as electronics, sensors and biomedical devices. [2,5-9] The efficient and robust creation of nanowires with functional nanocomponents and nanosolder segments could serve as a basic building block for nanoelectronic integration. [10-12] Nanoscale solders can be electrodeposited on metallic nanowires grown in nanoporous membranes. [13-16] Upton heating, the metallurgical reaction between the solder wire segment and metallic wire segment results in the formation of intermetallic compounds (IMC) that serve as the mechanical bonding between the solder segment and the functional element (i.e., metal base segment). [2]

Soldering is a well-recognized metallurgical joining method for bonding solder to a base metal. Interfacial reactions at the solder joints are key reliability factors in the fabrication of electronic products. Typically, a thin and uniform IMC layer is required for good bonding. A thick IMC layer between the solder and base metal may degrade the reliability of the solder joints because of the inherent brittle nature and the tendency to generate structural defects and stresses caused by structure and property (e.g., elastic modulus, thermal expansion) mismatches between the IMC and base metal. [17,18] Therefore, a deep fundamental understanding of the interfacial reactions at the solder joints and phase evolution in the solder interconnections is essential to developing reliable solder interconnections. [19-22]

The Cu–Sn system is one of the widely used metallurgical systems for system integration and electronic packaging because of its easy formation of Cu–Sn IMCs that serve as the mechanical bonding between the Sn-based solder and the copper pad of a printed circuit board. The solid-state growth of Cu-Sn IMCs in the form of bulk materials has been studied extensively. The miniaturization of electronics

ACCEPTED MANUSCRIPT

AIP Publishing

This manuscript was accepted by J. Appl. Phys. Click here to see the version of record.

devices into the nanometer scale requires efficient and effective methods for joining and interconnecting individual nanostructured units. [6,23] Fundamental understanding of the interfacial reactions including wetting, dissolution, reactive phase formation between the nanosolder and functional nano-components is still very limited.

Recently, the interfacial reaction and associated phase evolution in two-segment Cu-Sn nanowires has been studied. [24, 25] However in real application it is more often that the solder element is sandwiched between two base metals (Cu/Sn/Cu) or the substrate being placed between two solder particles (Sn/Cu/Sn). [3,26-28] For the case of the Cu/Sn/Cu configuration, Sn diffuses toward the two Cu segments at each side and Cu diffuses into the Sn segment in between. For the case of the Sn/Cu/Sn configuration, Cu diffuses out towards to the two Sn segments at each side and reacts with incoming diffusing Sn from both sides during the soldering reaction. Thus the difference in symmetry as compared to the two-segmented Cu/Sn system raises fundamental interests of understanding the soldering reaction such as the interdiffusion void growth and IMC formation in the three-segmented Cu/Sn/Cn and Sn/Cu/Sn nanowires. In this study, the soldering reaction of a segment of pure Sn sandwiched between two segments of Cu base metal as well as a segment of Cu base metal sandwiched between two segments of Sn is comparatively investigated by in-situ transmission electron microscopy (TEM). Our results demonstrate that the interface reaction at the solder joints depend on the configuration of the sandwiched structures and differ significantly in the key features of the soldering reactions in the Sn/Cu/Sn and Cu/Sn/Cu nanowires including IMC formation, microstructure evolution, and growth of the Kirkendall voids.

ACCEPTED MANUSCRIPT

2. Experimental

The Cu-Sn-Cu and Sn-Cu-Sn three-segmented nanowires were fabricated by room-temperature sequential electrodeposition assisted with polycarbonate nanoporous membrane templates (Whatman). Cu was deposited using a commercial Cu plating electrolyte (Cu U-bath RTU, Technic, Inc) with the current controlled at 2 mA/cm^2. The Sn layer was electroplated by commercial Sn plating electrolyte (Sn concentrate with make-up solutions, Technic, Inc.) with the current controlled at 18 mA/cm^2. After the

AIP Publishing

This manuscript was accepted by J. Appl. Phys. Click here to see the version of record.

electroplating, the polycarbonate membrane was dissolved in dichloromethane to release the nanowires into the solvent. Details of the synthesis of the nanosolders can be found from previous work. [13,14,25] The as-prepared segmented nanowires were kept as a suspension in ethanol. TEM samples were prepared by the powder sample preparation method with ultrasonic dispersion followed with drop casting onto a lacey carbon film supported by Mo grid, which was then mounted onto a Gatan heating holder with rapid heating capability using a Gatan hot-stage temperature controller. In-situ TEM and scanning TEM (STEM) observations of the metallurgical reaction in the three-segment nanowires were performed using a JEOL JEM2100F operated at 200 kV equipped with an x-ray energy dispersive spectrometer (XEDS) (Oxford Energy TEM 250).

3. Results and Discussion

Cu and Sn segments are sequentially electrodeposited in the form of nanowires for studying the metallurgical reaction with Sn as the soldering material between two Cu segments or one Cu segment between two sections of the soldering element. Fig. 1(a) shows a backscattered scanning electron microscope (SEM) image of the as-synthesized Sn-Cu-Sn nanowires and the inset is a magnified SEM image of a single nanowire. Because Sn has a larger atomic number than Cu, the bright segment at the right end corresponds to the Sn segment, the slightly darker region in the middle is the Cu segment, and the brighter segment on the left corresponds to the Sn segment. These nanowires were fabricated by electroplating with the commercially available nanoporous templates. These templates are not electrical conductive materials. To enable the electroplating reaction an electrically conductive silver layer was evaporated to cover the surface of the nanopores and the bottom side of the template also has to be sealed by an electrically conductive layer. This led to in a smaller size of the nanopores at the bottom side than that at the top side of the template. The inhomogeneous template pore size resulted in fabricated nanowires with one end coarser than the other. The coarse and find ends of the nanowires cause difference in the SEM image contrast. The contrast of backscattered scanning electron images comes from the ability of the atoms to reflect and scatter the incident electrons. The coarse end have more

ACCEPTED MANUSCRIPT

AIP Publishing

This manuscript was accepted by J. Appl. Phys. Click here to see the version of record.

electrons that are backscattered into the SEM detector as compared to the fine end of the nanowire. Therefore, the coarse end appears brighter than the fine end in the SEM image. Fig. 1(b) shows a STEM dark field image of an as-synthesized Sn-Cu-Sn three-segmented nanowire. The corresponding EDS Cu and Sn elemental maps of the nanowire are shown in Figs. 1(c, d), from which the Cu and Sn segments can be easily identified. Fig. 1(e) shows a backscattered SEM image of as-synthesized Cu-Sn-Cu three-segmented nanowires, the inset is a magnified SEM image of the nanowires, which shows strong contrast for the Sn segment in the middle while slightly weaker contrast for the two Cu segments at each side. Fig. 1(f) shows a STEM bright field image of an as-synthesized Cu-Sn-Cu three-segmented nanowire. The corresponding EDS elemental mapping is shown in Figs. 1(g, h), from which it is easy to identify the two Cu segments and the Sn segment in between. Our TEM examination shows that the three-segment Cu-Sn-Cu and Sn-Cu-Sn nanowires fabricated by electrodeposition do not have any specific crystal orientation preference. From the elemental mapping of the as-prepared nanowires shown in Figs. 1(c, d) and Figs. 1(g, h), we can see the Cu/Sn interfaces for both Cu-Sn-Cu and Sn-Cu-Sn nanowires are all inclined. The tilt angle of the interfaces can be different for different nanowires.

To investigate the IMC formation along with the Kirkendall void growth during the soldering reaction, a single nanowire is used for in-situ heating TEM observations. Fig. 2 shows the morphological evolution of a Sn-Cu-Sn nanowire while it is being heated from room temperature (RT) to 236.5 °C. The dashed lines in Fig. 2 denote the original interface regions between the Cu segment and the two Sn segments at each side, as known from the STEM EDS Cu and Sn maps of this nanowire shown in Figs. 1(c, d), with the Cu segment in the middle of the nanowire between the two segments of Sn on the left and right side. The Sn segment on the left has a larger diameter as compared to the one on the right. The nanowire has no obvious changes until it is being heated to ~174.4 °C, at which a void appears in the Cu segment. This void grows as the temperature increases, as shown in the TEM images at 198.1 °C, 204.4 °C and 205.7 °C respectively. The Cu_6Cu_5 formation during the heating process transforms the two original Cu/Sn interfaces to two Cu_6Sn_5/Cu interfaces that propagate toward the Cu segment in the middle and the two Cu_6Sn_5/Sn interfaces that move to the two Sn segments with the continued IMC growth. The void

ACCEPTED MANUSCRIPT

AIP Publishing

This manuscript was accepted by J. Appl. Phys. Click here to see the version of record.

shown in Fig. 2 is actually close to the Cu_6Sn_5/Cu interface on the right. The close proximity of the Kirkendall voids with the IMC/Cu interface is confirmed by both the composition measurement with EDS and structure analysis with electron diffraction. The Kirkendall void formation in the Cu segment is due to the mass loss because the diffusion of Cu atoms out of the segment is faster than the diffusion of Sn atoms into the Cu region. With continued heating and increase of temperature, the void shrinks and shifts to the left, as indicated in the TEM images at 206.3 ℃. The intermetallic reaction and IMC formation in the Cu segment leads to substantial volume expansion due to the molar volume difference between the reaction product and the parent metal ($\Delta V=V(Cu_6Sn_5)-6V(Cu)=75.4cm^3/mol$). In Sn-Cu-Sn three-segmented nanowires, Cu diffuses out of the segment towards the two neighboring Sn segments. The faster outward diffusion of Cu than the inwards diffusion of Sn favors the void formation in the Cu segment away from the IMC/Cu interface. As shown in the TEM image of the nanowire at 206.6 ℃ in Fig. 2, the local area around the void appears brighter as compared to other areas, suggesting that Cu is gradually depleted from this region. In addition, the in-situ TEM images in Fig. 2 show that the voids in the Cu segment migrate away from the IMC/Cu interface, which is in the opposite direction from the diffusion of Cu atoms to the IMC/Cu interface for the IMC growth, further supporting the diffusion induced mass loss for voiding in the Cu segment.

The incoming Sn atoms from the two Sn segments allows for continued Cu_6Sn_5 growth by reacting with the remaining Cu in this region, and the resulting volume expansion associated with the IMC formation gradually refills the void. As shown in the time-sequence TEM images obtained from the nanowire at 206.6 ℃ for 108 s, 150 s, 181 s, and 289 s in Fig. 2, the continued IMC growth leads to the void shrinkage and eventual disappearance. With further heating and increased temperature above 206.6 ℃, there are no noticeable changes for the nanowire. The temperature is then further increased above the melting the melting point of Sn to investigate how Cu_6Sn_5 may interact with remnant Sn at elevated temperature. At 236.5 ℃ and above, Sn melts as known from the electron diffraction taken from the Sn segment. It should be noted that there is no solid Cu/liquid Sn contact involved because the temperature is increased gradually and slowly and the temperatures and the isothermal holding time

ACCEPTED MANUSCRIPT

AIP Publishing

This manuscript was accepted by J. Appl. Phys. Click here to see the version of record.

intervals at each temperature are given in Fig. 2. Therefore, the intermetallic reaction occurs way before reaching the melting point of Sn. All the soldering reaction and the associated bulging and Kirkendall voiding shown in Fig. 2 occur in the solid state until the temperature reaches 236 ℃.

Figs. 3(a-d) show the TEM image and the corresponding EDS Cu and Sn elemental maps of the reacted nanowire shown in Fig. 2 with the temperature held at 236.5 ℃. It can be seen that Sn distributes along the whole nanowire while Cu diffuses and reaches to the left end of the nanowire. There is remnant Sn left at the right end of the nanowire. To gain more quantitative information about the chemical composition, EDS linescan along the length direction of the reacted nanowire is acquired from the nanowire with its temperature held at 236.5 ℃. The plotted Cu and Sn concentration profiles obtained from the EDS linescan is shown in Fig. 3(d). The EDS elemental mapping and line scan shown in Fig. 3 were taken from the molten Sn at the elevated temperature. Figs. 3(b, c, and d) correspond to the state when Sn just reached the molten state. As known from the concentration profile along the length direction of the wire at 236.5 °C (Fig. 3(d)), the segment from x_2 to the right end of the nanowire still remains as pure Sn after reaching the liquid state. With the prolonged heating and temperature ramping to 299 °C, the length of the remnant Sn segment increased slightly, as indicated by the slight left shift of position x_6 in Fig. 3(e) relative to x_2 in Fig. 3(d), indicating that some IMC adjacent to the molten Sn was dissolved into the molten Sn at the IMC/Sn interface during the heating process. Near the left end there is a segment rich in Sn which ranges from the most left end (x=0) to the position as indicated by the dash line x_1. This Sn rich region is probably Sn rich liquid phase at the temperature of 236.5 ℃. [29,30] Following the Sn rich segment the composition features a plateau with Cu slightly over 50 at%. It corresponds to the η-Cu_6Sn_5 intermetallic phase as identified by electron diffraction shown later in Fig. 4. The concentration line scan profile acquired at 236.5 ℃ as indicated in Fig. 3(d) shows that the intermetallic phase formed is Cu_6Sn_5, which leads to the volume expansion and bulging. Therefore, the void formation in the Cu segment rather than in the Cu_6Sn_5 segment (Fig. 2) must be due to the fast outward-diffusion of Cu, which results in the mass depletion in the local region of the Cu segment. In other words, the void formation in the Cu

ACCEPTED MANUSCRIPT

AIP Publishing

This manuscript was accepted by J. Appl. Phys. Click here to see the version of record.

segment is induced by the faster outward diffusion of Cu than the inward-diffusion of Sn. Such Kirkendall voiding in the Cu segment has been repeatedly observed from in-situ TEM experiments. [24,25,31] The resulting η-Cu_6Sn_5 segment ranges from position x_1 to x_2 as marked by the dash lines in Fig. 3(d). From x_2 to the right end of the nanowire (x = 3.88 μm), it is mostly Sn with approximately 10 at% Cu. At this temperature, Sn is in a molten state as identified by the electron diffraction shown later in Fig. 4. Liquid Sn can dissolve slightly Cu in the IMC at the molten Sn/Cu_6Sn_5 interface, as evidenced by the slight shift of the Sn/Cu_6Sn_5 interface toward the right end by comparing Figs. 3(d and e). This is also consistent with the Cu-Sn phase diagram[32]. Fig. 3 also shows that there is no further intermetallic reactions at the temperatures (236.5 °C and 299 °C) above the melting point of Sn because Cu was completely consumed at the lower temperature shown in Fig. 2.

Cu diffuses towards both the coarse and thin ends of the nanowires for the reacted Sn-Cu-Sn couples although it indeed appears (Fig. 3) that Cu diffuses to reach the coarse end of the nanowire while the thin end remains nearly pure Sn. It should be noted that the Sn segment on the right is a lot longer than the Sn segment on the left before heating (shown in Fig. 2). Due to the one-dimensional confined geometry of the nanowire, the diffusion direction of Cu and Sn atoms is largely confined along the length direction of the nanowire and we have to take account of the diffusion distance in order to reach to the two ends of the nanowire. We can take the initial Sn/Cu interface as the diffusion front of Cu to begin with, the diffusion distance for Cu to reach the coarse end of the nanowire is the length of the Sn segment on the left and the diffusion distance for Cu to reach the fine end of the nanowire equals the length of the Sn segment on the right side (see Fig. 2, RT). Larger distance requires longer time for atoms to diffuse through with the same diffusion rate (at a constant temperature). In our symmetrical diffusion couples with Cu diffusion towards both the left and right ends of the nanowire, the diffusion distance of Cu should be equal for both sides. Under the reaction stage shown in Fig. 3, Cu has reached the coarse end of the Sn segment on the left while still has not yet reached the fine end of the Sn segment on the right because of its larger length. As a result, the right end of the nanowire appears as pure Sn in the EDS mapping shown in Fig. 3.

ACCEPTED MANUSCRIPT

AIP Publishing

This manuscript was accepted by J. Appl. Phys. Click here to see the version of record.

The solder reflow temperatures in industry application often go slightly above the melting point of Sn to ensure good bonding,[33,34] it is therefore necessary to check any structural and compositional changes in the IMCs above the melting point of Sn. We therefore examine the structure and composition of the nanowires at the elevated temperature up to 299 °C, which may be of relevance for the potential application in high temperature soldering. The Cu and Sn concentration profiles obtained from STEM EDS linescan acquired at 299 ℃ is shown in Fig. 3(e). From x=0 to x_3 the segment is Sn rich. The composition corresponds to η-Cu_6Sn_5 ranging from x_3 to x_4 and from x_5 to x_6. There is a narrow segment rich in Sn positioned from x_4 to x_5 as indicated by the dash lines in Fig. 3(e). This is a "spike" with the high concentration of Sn ranging from x_4 to x_5. From x_6 to the right end of the nanowire (x = 3.88 μm) it is molten Sn with a minor amount of Cu. By comparing the concentration profiles taken at 236.5 ℃ and 299 ℃, the temperature induced growth or shrinkage of the phases along the nanowire can be revealed. The position of x_3 shifts to the left side of the wire as compared to x_1, which indicates that the Sn rich segment shortens because Sn diffuses towards the right end of the nanowire. The position of x_6 shifts toward the left side as compared to the position of x_2, which indicates that the length of the molten Sn region increases. Sn atoms from the Sn-rich region (from x=0 to x_1) on the left side diffuse through the solid-state η-Cu_6Sn_5 to support the growth of molten liquid Sn. The "spike" region has a higher concentration of Sn as compared to the surrounding η-Cu_6Sn_5 phase, it is highly possible that incoming Sn reacts with η-Cu_6Sn_5 and form Sn-rich molten liquid according to the Cu-Sn phase diagram. [32,35] This eutectic reaction occurs at 227 ℃, slightly below the melting point of pure Sn. Especially when the temperature rises beyond the melting point, the diffusivity of Sn atoms in η-Cu_6Sn_5 solid phase also increases. We can think of the mass flow of both Cu and Sn along one dimension with concentration fluctuation, when there is sufficient amount of Sn, the eutectic reaction occurs and Sn rich liquid nucleates at the local region (i.e., as pointed by the black arrow in Fig. 3 (d)). Once a stabilized liquid nucleus forms, it will grow and dissolve more Sn (i.e., the concentration "spike" as denoted by the dash line x_4 and x_5 in Fig. 4 (e)), and meanwhile Cu will be segregated from the liquid and diffuses into the

ACCEPTED MANUSCRIPT

AIP Publishing

This manuscript was accepted by J. Appl. Phys. Click here to see the version of record.

adjacent solid η-Cu_6Sn_5 gains. The supply of Sn atoms is from the most left side of the Sn-rich region (i.e., from the most left to x_1) for the eutectic liquid phase to grow.

The crystal structure and phases of the reacted nanowire with its temperature held at 299 ℃ are examined by electron diffraction as shown in Fig. 4. Figs. 4(b, c, d) are selected-area electron diffraction (SAED) patterns obtained from areas "1", "2" and "3" as encircled by dash red circles in Fig. 4(a). Areas "1" and "2" are the η-Cu_6Sn_5 phase with different orientations of $[11\bar{1}]$ and $[24\bar{1}]$, indicating that the soldering reaction has the strong tendency to form polycrystalline η-Cu_6Sn_5 although the parent nanowire has the single-crystalline segments of Cu and Sn. The formation of the polycrystalline η-Cu_6Sn_5 segment can be related to the multiple sites of nucleating the η-Cu_6Sn_5 grains in the parent Cu segment. The diffraction pattern from area "3" has diffuse rings, which confirm the molten state of the Sn-rich segment at the elevated temperature of 299 ℃.

As compared to the Cu segment sandwiched by two segments of the soldering material of Sn shown above, one segment of Sn connecting two metallic base parts is more common in real application. Therefore, Cu-Sn-Cu three-segmented nanowires are also studied by in-situ TEM to observe the IMC formation and void growth during the soldering reaction. As known from Fig. 2, the metallurgical reaction, especially the IMC growth, becomes completed mostly before reaching the melting point of Sn. Therefore, the temperature of the nanowires is held at the constant temperature of 200 ℃ for in-situ TEM observation of the morphological evolution and associated phase evolution. As shown in Fig. 5, the interfaces between the Cu and Sn segments before heating are marked by the red dash lines in the TEM image at 0 s according to the Cu and Sn elemental maps as shown in Figs. 1(g, h). At 123 s of the heating at 200 ℃, a Kirkendall void appears in the Cu segment on the right hand side. The Kirkendall void forms in the Cu segment due to the faster outward diffusion of Cu than the incoming diffusion of Sn. The void grows with time until it breaks the nanowire at 506 s. Meanwhile, there is another void appearing in the Cu segment on the left hand side at 380 s. This void grows larger over time until at 628 s. The void is then observed to shift to the left due to the net mass flow toward right, as shown in the TEM images of 628 s

ACCEPTED MANUSCRIPT

AIP Publishing

This manuscript was accepted by J. Appl. Phys. Click here to see the version of record.

and 751 s. The void continues to grow with time until it completely breaks the wire at 969 s. With the continued heating at 200 ℃, there is no noticeable change along the nanowire. The large void on the right does not shift because the complete breakage of the Cu segment by the void growth shuts off the supply of Cu and thus terminates the IMC growth. For the void on the right, the void shifts to the left, which is in the same direction as the IMC/Cu interface propagates toward the Cu segment. After the void growth completely breaks up the Cu segment, the void stays stationary over time, similar as the void on the right. Both of the voids shown in Fig. 5 are close to the Cu/IMC interfaces, as confirmed from the EDS and electron diffraction analysis (Figs. 6(d, e)). The in-situ TEM observation also shows that a particle (i.e., a bulge with slightly dark image contrast) nucleates and grows near the Cu/Sn interface region. To confirm it is a bulge rather than an embedded precipitate, the sample is tilted with rotation axis along the length direction of the nanowire. As shown in the last TEM image shown Fig. 5, the bulge is clearly visible near the interface of the Cu/Sn segment by tilting the sample. Because TEM imaging is a projection view of a 3D object, the 3D bulge is "invisible" from the planar-view in the time-sequence TEM images in Fig. 5. After the tilting around the axis along the length direction of the nanowire, the bulge becomes visible from the side view of the TEM imaging. As seen in Fig. 2, the areas showing locally darker contrast, as marked by the dashed red circles in Fig. 2 might come from the bulge formation in the Cu segment and near the Cu/Sn interface for the Sn-Cu-Sn couple. Similarly, the bulge formation also occurs for the Sn-Cu-Sn couple in the Cu segment, as shown in Fig. 5. It can be noted that the bulges seen in Fig. 2 are imaged in plan view, for which the TEM image contrast for the bulges is not as conspicuous as that shown in Fig. 5, where the bulge grows toward the side surface of the nanowire thereby allowing for a cross-sectional view. The comparative in-situ TEM observations indicate that the Sn-Cu-Sn couples tend to form more individual Cu_6Sn_5 bulges than the Cu-Sn-Cu couples because the Sn-Cu-Sn configuration provides more Sn to the Cu segment for the metallurgical reaction to form the Cu_6Sn_5 phase (Figs. 2-4). By contrast, Sn tends to spread into the two Cu segments for the Cu-Sn-Cu configuration, for which the metallurgical reaction results in the formation of the Cu-rich Cu_3Sn phase in addition to the Cu_6Sn_5 bulge (see Figs. 5-7).

ACCEPTED MANUSCRIPT

AIP Publishing

This manuscript was accepted by J. Appl. Phys. Click here to see the version of record.

To uncover the phase and structure of the reacted nanowire including the bulge, electron diffraction combined with chemical composition analysis is performed on the reacted nanowire with its temperature held at 200 °C. Figs. 6(b, c, d) are the SAED patterns obtained, respectively, from area "1", "2" and "3", as marked in Fig. 6(a). Areas "1", "2" and "3" are encircled by the red dash lines in Fig. 6(a). These diffraction patterns match well with the η-Cu_6Sn_5 structure with the different grain orientations, indicating the tendency to form polycrystalline η-Cu_6Sn_5. Fig. 6(e) is a magnified TEM image corresponding to the area indicated by the red dashed rectangle in Fig. 6(a). Fig. 6(f) is an SAED pattern obtained from the area encircled by the large red dashed circle shown in Fig. 6(e). The diffraction spots indicated by the red arrows are exclusively attributed to ε-Cu_3Sn,[32,35,36] which demonstrate the existence of ε-Cu_3Sn in addition to the η-Cu_6Sn_5 phase in the selected area. EDS spectra acquired in the STEM mode from the locations marked by the white crosses and labeled with numbers 1-8 as shown in Fig. 6(e) are plotted in Fig. 6(g). The spectra from bottom to top in Fig. 6(g) correspond to areas "1" to "8", respectively. The quantitative chemical composition of the different areas marked in Fig. 6(e) can be determined from the EDS spectra shown in Fig. 6(g). As shown in Fig. 6(e), spectra "1" and "2" are acquired from the left side of the Kirkendall void. Spectrum "1" has over 99 at. % Cu and spectrum "2" indicates over 92 at. % Cu. The nearly pure Cu confirms that the Kirkendall void forms preferentially in the Cu segment because of the faster outward diffusion of Cu than the inward diffusion of Sn. The continued growth of the void results in the breakage of the Cu segment with remnant Cu in the nanowire. Spectra from area "3", "4", "5" and "7" have the Cu content close to 75 at.%, which matches well with the composition in the ε-Cu_3Sn structure. The spectrum acquired from the bulge gives 62.8 at. % Cu, which is close to the composition of η-Cu_6Sn_5 and it confirms with the electron diffraction structural analysis from the bulge as shown in Fig. 6(b). The chemical composition from area "8" has 61.2 at. % Cu, which matches with the composition of the η-Cu_6Sn_5 phase. Fig. 6(d) shows the electron diffraction analysis to reveal that the void on the right is adjacent to the Cu_6Sn5 phase and Fig. 6(e) illustrate the EDS measurements that confirm the void on the left is between Cu and Cu_3Sn phase, which show the presence of pure Cu and 77at.% Cu (i.e., Cu_3Sn) surrounding the void on the left.

ACCEPTED MANUSCRIPT

AIP Publishing

This manuscript was accepted by J. Appl. Phys. Click here to see the version of record.

To further confirm the chemical composition, an EDS linescan along the length direction of the reacted nanowire with its temperature held at 200 ℃ is taken and the measured concentration profile is shown in Fig. 7. Five different compositions can be identified from the composition profile across the length direction of the nanowire. As shown in Fig. 7, remnant Cu with more than 95 at. % Cu in the two parent Cu segments (i.e., the solid solution of Sn in Cu) is indicated by the red arrows. Kirkendall voids with the concentration of both Cu and Sn drops to zero, locate between the Cu segment and IMC phases. The ε-Cu_3Sn region with approximately 75 at. % Cu is indicated by the black arrow in Fig. 7. The η-Cu_6Sn_5 segment with 60 at. % Cu is indicated by the purple arrow in Fig. 7. There is a "spike" of the high concentration of Sn in the η-Cu_6Sn_5 region. This is due to the remnant Sn from the parent Sn segment.

Fig. 8 shows the schematic illustrations that summarize the key difference in the metallurgical reactions of the sandwiched structures of the three-segmented Cu/Sn/Cu and Sn/Cu/Sn nanowires. For the three-segment Sn/Cu/Sn nanowires (Figs. 8(a-c)), our in-situ TEM analyses (Figs. 2-4) demonstrate that there is no ε-Cu_3Sn formation from the metallurgical reaction. The absence of the ε-Cu_3Sn phase can be attributed to the relative shortage of the supply of Cu as compared to Sn. Kirkendall void formation occurs initially in the parent Cu segment. The incoming diffusing Sn atoms from the two Sn segments to the sandwiched Cu segment can subsequently refill the void in the Cu segment. These incoming Sn atoms react with Cu and form multiple grains of η-Cu_6Sn_5 and the whole wire only has one single intermetallic phase of η-Cu_6Sn_5 from the metallurgical reaction. With continued heating at temperature slightly above the melting point of Sn, there is Sn-rich liquid phase formed between the η-Cu_6Sn_5 grains. The presence of the Sn-rich liquid phase can pose significant threat on the mechanical properties of the joints. Our further TEM analyses show that this Sn-rich liquid phase does not transform to any IMC phases after the sample is cooled to room temperature because of the lack of Cu for the IMC formation.

For the three-segmented Cu/Sn/Cu nanowires (Figs. 8(d-f)), our in-situ TEM analyses shown in Figs. 5-7 demonstrate that the metallurgical reaction results in the intermetallic phases of multiple grains of both Cu_3Sn and Cu_6Sn_5 with a bulge of the single-crystal Cu_6Sn_5 grain formed on the Cu_3Sn segment. Kirkendall void formation occurs in each parent Cu segment. The growth of the voids in the two Cu

ACCEPTED MANUSCRIPT

AIP Publishing

This manuscript was accepted by J. Appl. Phys. Click here to see the version of record.

segments leads to the breakage of the nanowire, which may pose a threat to the integrity and mechanical strength and reliability of the joints. For the Cu/Sn/Cu configuration, adding a barrier layer between the Cu/Sn to reduce the diffusion rate of Cu into Sn may be necessary for reducing the growth of the Kirkendall voids in the Cu segment. Optimizing the relative lengths of the segments of Cu and Sn along with the temperature and time above or near the melting point of Sn might be essential to avoid the formation of the liquid phase in the intermetallic phase and overgrowth of the Kirkendall voids in the segments of the base metal. The in-situ TEM results shown above provide dynamic information of the Cu/Sn metallurgical reaction including Kirkendall voiding, IMC formation, and bulging. The in-situ TEM observations show that the IMC growth can lead to the shrinkage and disappearance of Kirkendall voids (Fig. 2). On the other hand, the complete breakage of the nanowire with the void growth can shut off the supply of Cu atoms and thus terminate the IMC growth (Fig. 5). This differs from the bulk Cu/Sn system, in which the Kirkendall void formation may not significantly slow down the IMC growth because inter-diffusion can still occur through the surrounding area of the void. Our in-situ TEM observations also reveal the temporal and spatial dependence of the IMC phases on the geometrical configuration of the solder and base metal. The Sn/Cu/Cu configuration forms the Cu_6Sn_5 phase while the Cu/Sn/Cu configuration results in the intermetallic phases of both Cu_6Sn_5 and Cu_3Sn because the latter configuration provides more Cu to form the Cu-rich Cu_3Sn phase. From the in-situ TEM observations, we find that bulging occurs mainly in the region close to the Cu/Cu_6Sn_5 interface. The temporal and spatial movement of the Cu/IMC interface may result in the formation of multiple bulges over time (Fig. 2). Such dynamic information cannot be readily obtained from post-mortem TEM observations, even with the ex-situ experiments performed under the same reaction condition.

4. Conclusions

In-situ TEM has been employed to study the soldering reaction of three-segmented Sn/Cu/Sn and Cu/Sn/Cu diffusion couples to mimic the real life application of these sandwiched nanowire structures. For the Sn/Cu/Sn diffusion couple, there is no ε-Cu_3Sn formation from the intermetallic reactions due to

ACCEPTED MANUSCRIPT

AIP Publishing

This manuscript was accepted by J. Appl. Phys. Click here to see the version of record.

the relative short supply of Cu as compared to Sn. The initially formed Kirkendall voids in the Cu segment can be subsequently refilled by the volume expansion associated with the IMC growth. The incoming Sn atoms react with the Cu segment to form η-Cu_6Sn_5 and the entire nanowire has only one single intermetallic phase of η-Cu_6Sn_5. With continued heating at temperature slightly above the melting point of Sn there is Sn rich liquid phase formed between the η-Cu_6Sn_5 grains. For the metallurgical reaction in the Cu/Sn/Cu diffusion couple, the resulting intermetallic phases consist of both Cu_3Sn and Cu_6Sn_5, and a bulge with the single-crystalline Cu_6Sn_5 grain formed on the Cu_3Sn segment. Kirkendall void formation occurs in each of the parent Cu segments and the continued void growth results in the breakage of the reacted nanowire and thus the termination of the IMC growth.

Acknowledgement:

This work was supported by the National Science Foundation under NSF Collaborative Research Award Grant CMMI-1233806. Research carried out in part at the Center for Functional Nanomaterials, Brookhaven National Laboratory, which is supported by the U.S. Department of Energy, Office of Basic Energy Sciences, under Contract No. DE-SC0012704.

ACCEPTED MANUSCRIPT

AIP Publishing

This manuscript was accepted by J. Appl. Phys. Click here to see the version of record.

References:

1 Y. Zhou and A. Hu, Open Surface Science Journal **3,** 32 (2011).
2 X. Li, F. Gao, and Z. Gu, Open Surface Science Journal **3,** 91 (2011).
3 A. J. Call, E. B. Cohen, D. Minier, W. Sauter, D. B. Stone, and E. W. Tremble, (Google Patents, 2015).
4 R.-Z. Li, A. Hu, D. Bridges, T. Zhang, K. D. Oakes, R. Peng, U. Tumuluri, Z. Wu, and Z. Feng, Nanoscale **7,** 7368 (2015).
5 W. Zhou, X. Dai, T.-M. Fu, C. Xie, J. Liu, and C. M. Lieber, Nano Letters **14,** 1614 (2014).
6 T.-M. Fu, X. Duan, Z. Jiang, X. Dai, P. Xie, Z. Cheng, and C. M. Lieber, Proceedings of the National Academy of Sciences **111,** 1259 (2014).
7 X. Duan, R. Gao, P. Xie, T. Cohen-Karni, Q. Qing, H. S. Choe, B. Tian, X. Jiang, and C. M. Lieber, Nature nanotechnology **7,** 174 (2012).
8 Z. Fan, J. C. Ho, T. Takahashi, R. Yerushalmi, K. Takei, A. C. Ford, Y. L. Chueh, and A. Javey, Advanced Materials **21,** 3730 (2009).
9 K.-I. Chen, B.-R. Li, and Y.-T. Chen, Nano Today **6,** 131 (2011).
10 Y. Lin and W. Jian, Nano Letters **8,** 3146 (2008).
11 Y. Peng, T. Cullis, and B. Inkson, Nano Letters **9**, 91 (2008).
12 Q. Cui, K. Rajathurai, W. Jia, X. Li, F. Gao, Y. Lei, and Z. Gu, The Journal of Physical Chemistry C **114,** 21938 (2010).
13 Z. Gu, H. Ye, D. Smirnova, D. Small, and D. H. Gracias, Small **2,** 225 (2006).
14 F. Gao, S. Mukherjee, Q. Cui, and Z. Gu, The Journal of Physical Chemistry C **113,** 9546 (2009).
15 M. Shaygan, T. Gemming, V. Bezugly, G. Cuniberti, J.-S. Lee, and M. Meyyappan, J. Phys. Chem. C. **118,** 15061 (2014).
16 B. Nikoobakht, X. Wang, A. Herzing, and J. Shi, Chemical Society Reviews **42,** 342 (2013).
17 K. N. Tu, *Solder joint technology* (Springer, 2007).
18 F. Che and J. H. Pang, Journal of Alloys and Compounds **541,** 6 (2012).
19 T.-C. Liu, C.-M. Liu, Y.-S. Huang, C. Chen, and K.-N. Tu, Scripta Materialia **68,** 241 (2013).
20 Q. Li and Y. Chan, Journal of Alloys and Compounds **567,** 47 (2013).
21 L. M. Lee and A. A. Mohamad, Advances in Materials Science and Engineering **2013** (2013).
22 A. Paul, C. Ghosh, and W. Boettinger, Metallurgical and Materials Transactions A **42,** 952 (2011).
23 H. Zhang, J. Zhang, Q. Lan, H. Ma, K. Qu, B. J. Inkson, N. J. Mellors, D. Xue, and Y. Peng, Nanotechnology **25,** 425301 (2014).
24 Q. Yin, F. Gao, Z. Gu, J. Wang, E. A. Stach, and G. Zhou, Acta Materialia **125,** 136 (2017).
25 Q. Yin, F. Gao, Z. Gu, E. A. Stach, and G. Zhou, Nanoscale **7,** 4984 (2015).
26 J. Li, P. Agyakwa, and C. Johnson, Acta Materialia **59,** 1198 (2011).
27 L. Tsao, R. Wu, T.-H. Cheng, K.-H. Fan, and R. Chen, Materials & Design **50,** 774 (2013).
28 C. Liu, J. Chen, Y. Chuang, L. Ke, and S. Wang, Applied Physics Letters **90,** 112114 (2007).
29 Q. Yin, F. Gao, J. Wang, Z. Gu, E. A. Stach, and G. Zhou, Journal of Materials Research **32,** 1194 (2017).
30 A. Munding, H. Hübner, A. Kaiser, S. Penka, P. Benkart, and E. Kohn, in *Wafer Level 3-D ICs Process Technology* (Springer, 2008), p. 1.
31 Q. Yin, F. Gao, Z. Gu, E. A. Stach, and G. Zhou, Microscopy and Microanalysis **21,** 943 (2015).
32 N. Saunders and A. Miodownik, Bulletin of Alloy Phase Diagrams **11,** 278 (1990).
33 Z. Zhang and G.-Q. Lu, IEEE Transactions on electronics packaging manufacturing **25,** 279 (2002).
34 K. Kim, S. Huh, and K. Suganuma, Journal of Alloys and compounds **352,** 226 (2003).
35 D. Li, P. Franke, S. Fürtauer, D. Cupid, and H. Flandorfer, Intermetallics **34,** 148 (2013).
36 P. Brooks and E. Gillam, Acta Metallurgica **18,** 1181 (1970).

ACCEPTED MANUSCRIPT

AIP Publishing

This manuscript was accepted by J. Appl. Phys. Click here to see the version of record.

Figure Caption:

Fig. 1 (a) SEM image of as-prepared Sn-Cu-Sn three-segmented nanowires, inset: zoom-in view; (b) STEM HAADF image of a single Sn-Cu-Sn nanowire; (c, d) STEM EDS Cu and Sn elemental maps of the nanowire shown in (b). (e) SEM image of as-prepared Cu-Sn-Cu three-segmented nanowires, inset: zoom-in view; (f) STEM BF image of a single Cu-Sn-Cu nanowire; (g, h) STEM EDS Cu and Sn elemental maps of the nanowire shown in (f).

Fig. 2. In-situ TEM observation of the morphological evolution of a Sn-Cu-Sn three-segmented nanowire upon heating from room temperature (RT) to 236.5 °C. The red dash lines indicate the locations of the Cu/Sn and Sn/Cu interfaces before heating and the red dashed circles denote the dark region where it might be Cu_6Sn_5 bulges.

Fig. 3. (a) TEM image of the Sn-Cu-Sn nanowire being heated at 236.5 ℃ and beyond this temperature (note that the nanowire shown here is the same one from the heat treatment shown in Fig. 2); (b, c) STEM EDS Cu and Sn elemental maps of the nanowire at 236.5 ℃ with the Cu map in red and the Sn map in green; (d, e) STEM XEDS elemental linecans along the length direction of the nanowire at 236.5 ℃ and 299 ℃ respectively.

Fig. 4. (a) BF TEM image of the Sn-Cu-Sn three-segmented nanowire being heated at 299 ℃; (b, c, d) SAED patterns obtained from areas “1”, “2”, “3” indicated in (a).

Fig. 5. In-situ TEM observation of the morphological evolution of a Cu-Sn-Cu three-segmented nanowire withhold at 200 ℃. The red dash lines indicate the locations of the Cu/Sn and Sn/Cu interfaces before heating.

ACCEPTED MANUSCRIPT

AIP Publishing

This manuscript was accepted by J. Appl. Phys. Click here to see the version of record.

Fig. 6: (a) BF-TEM image of the Cu-Sn-Cu nanowire being heated at 200 ℃ for 1360 s; (b) SAED obtained from the bulge (area “1”, as indicated by the red dashed circle in (a); (c, d) SAED patterns obtained from encircled area “2”, “3” indicated in (a); (e) Magnified TEM image of the area indicated by the red dashed rectangle in (a); (f) SAED obtained from the area denoted by the dash circle in (e); (g) EDS point spectra taken from the areas numbered in (e), the spectra from bottom to top correspond to areas “1” to “8” sequentially.

Fig 7: STEM EDS linescan showing the composition profile along the length direction of the Cu-Sn-Cu nanowire being held at 200 ℃ for 1360 s (shown in Fig. 6(a)).

Fig. 8 Schematic showing the metallurgical reactions in the three-segmented Sn/Cu/Sn (a, b, c); and Cu/Sn/Cu nanowires (d, e, f).

ACCEPTED MANUSCRIPT

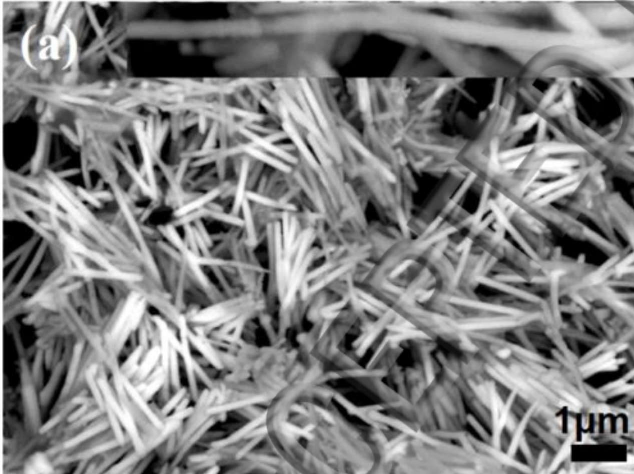
(a)
1μm

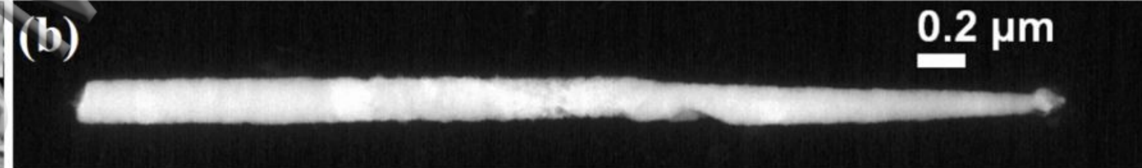
(b)
0.2 μm

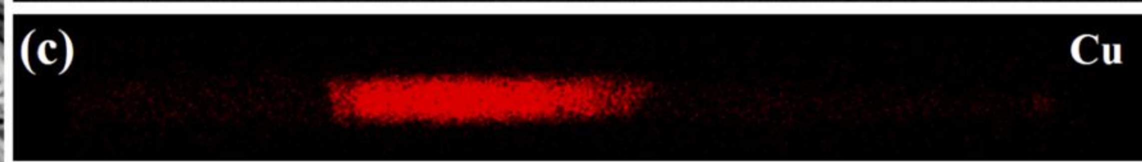
(c)
Cu

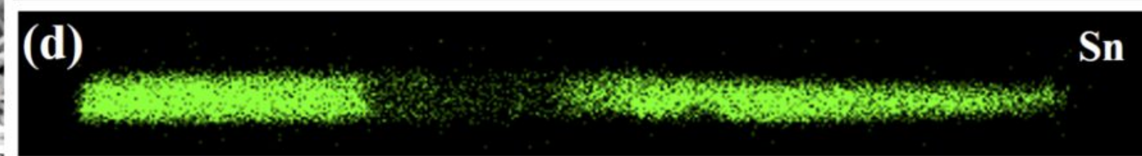
(d)
Sn

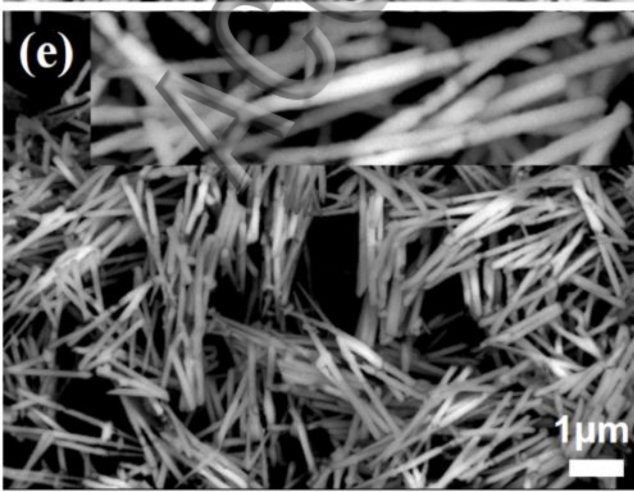
(e)
1μm

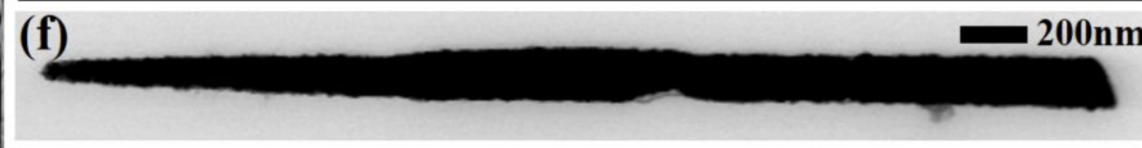
(f)
200nm

(g)
Cu

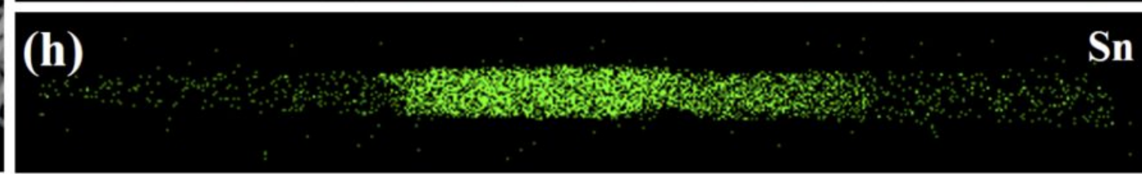
(h)
Sn

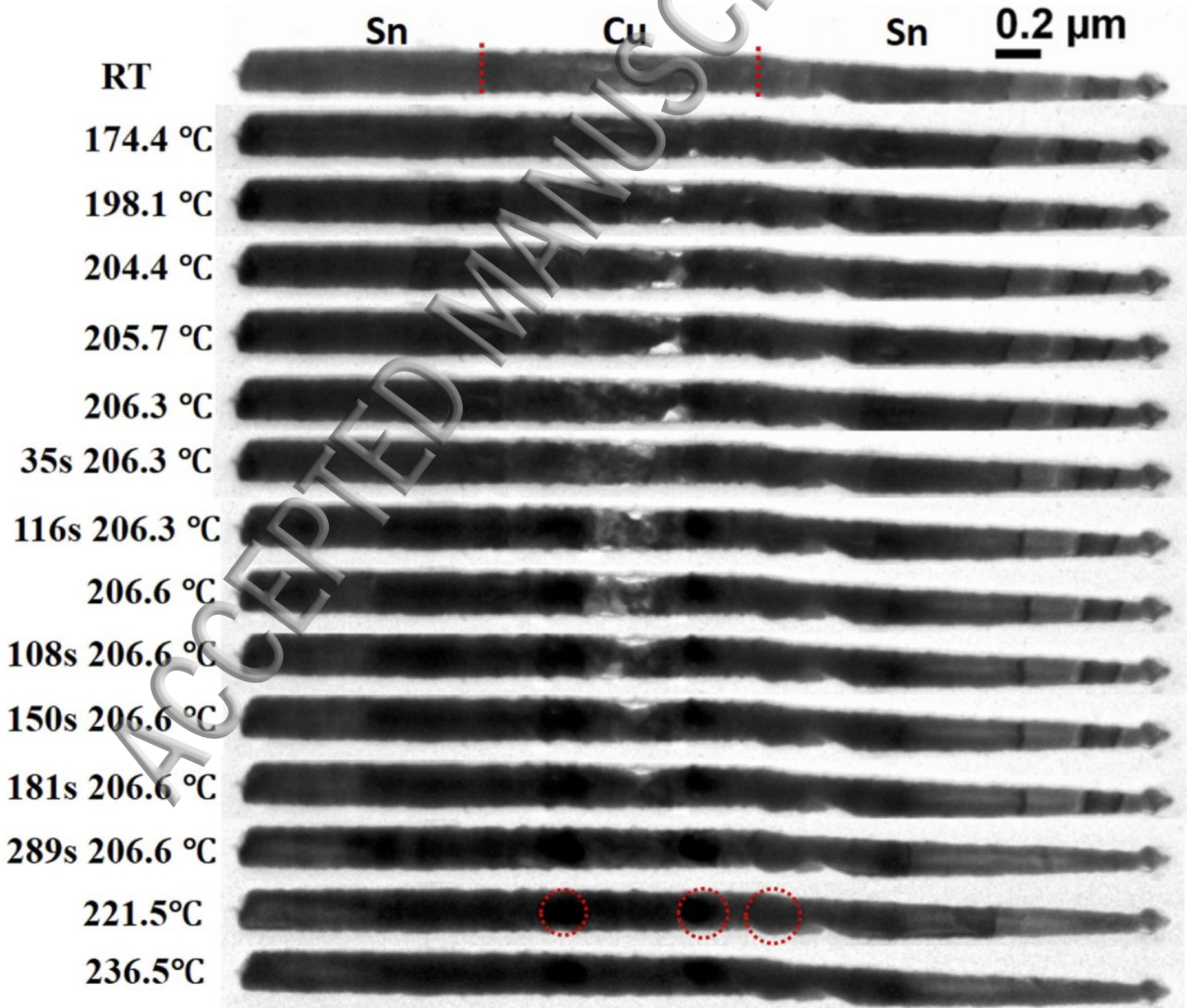

ACCEPTED MANUSCRIPT

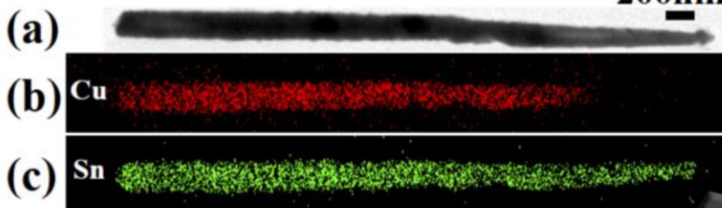

ACCEPTED MA

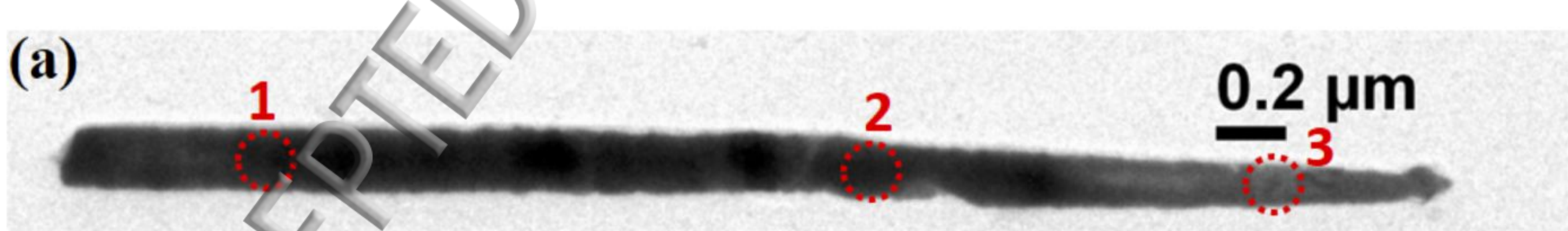

ACCEPTED

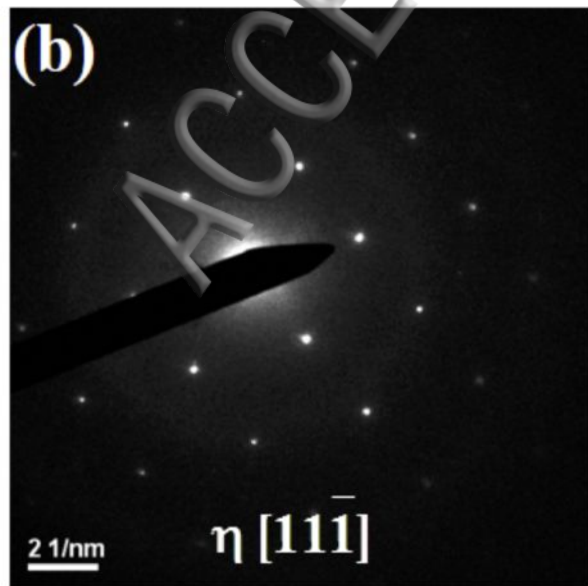

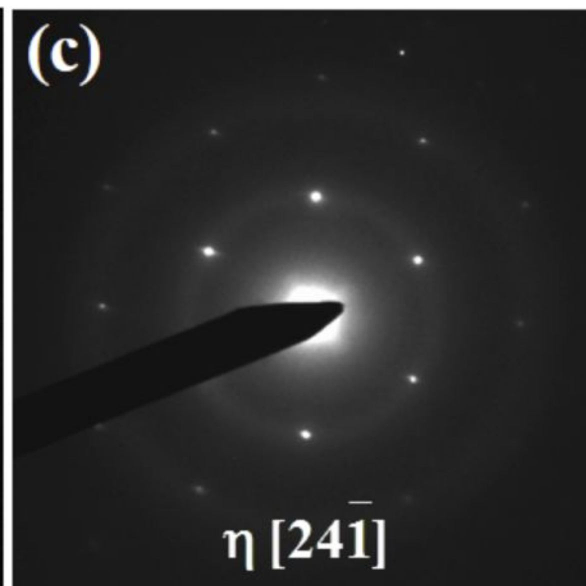

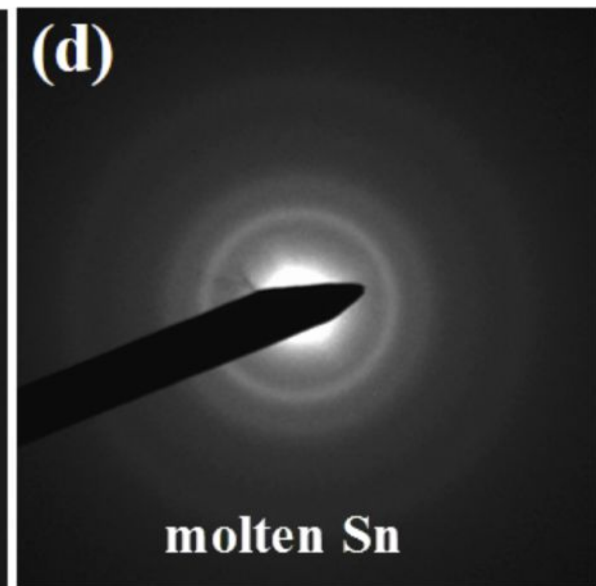

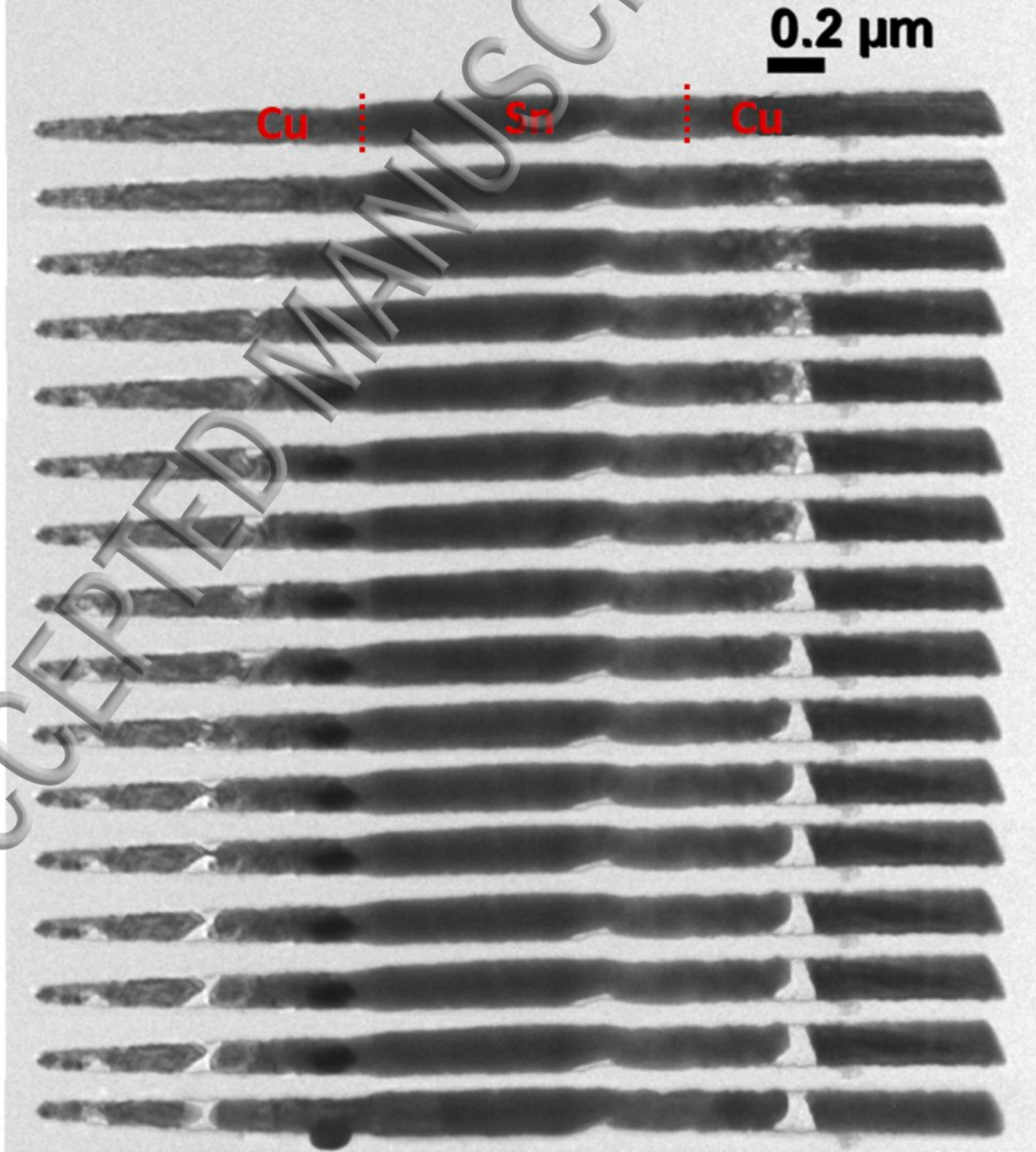

ACCEPTED MANUSCRIPT

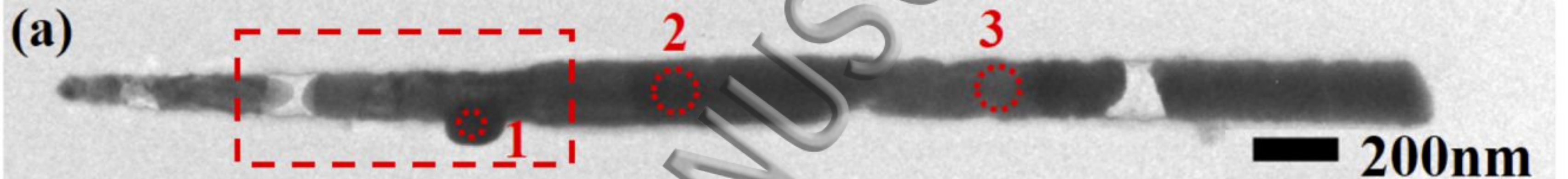

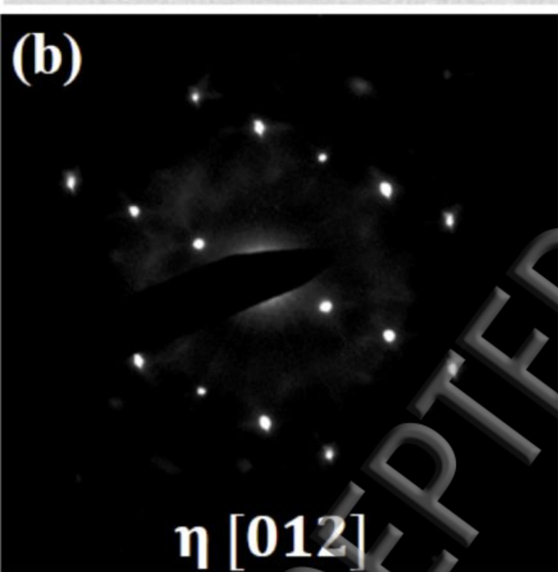

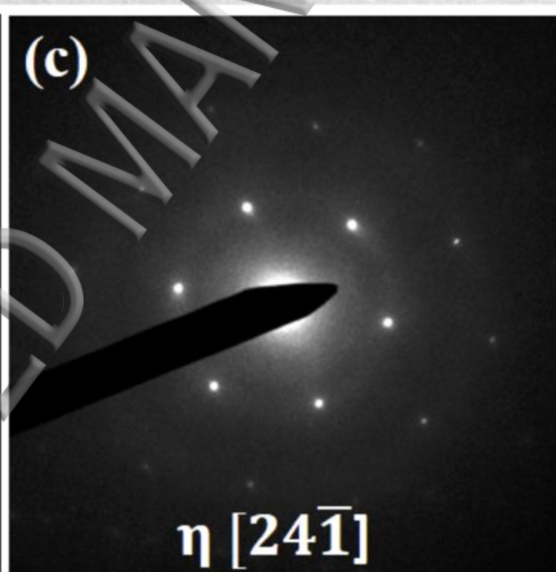

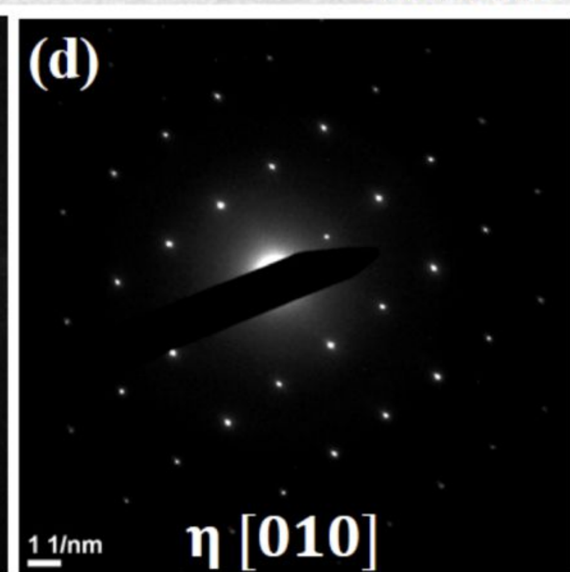

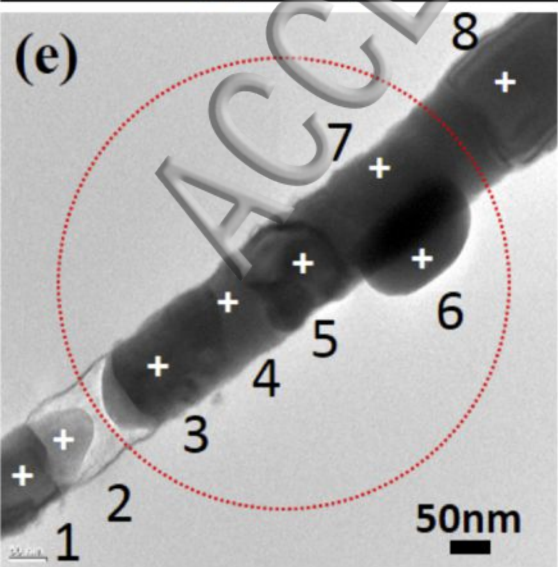

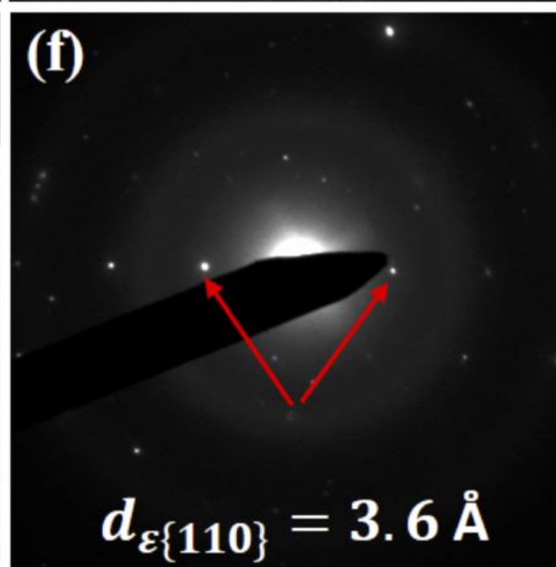

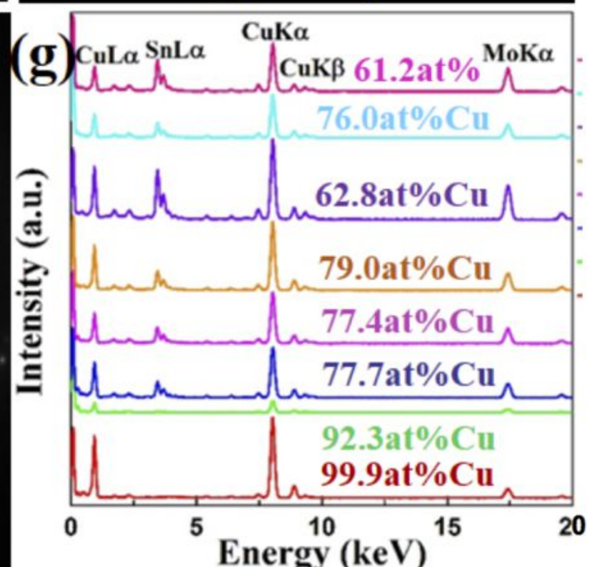

ACCEPTED MANUSCRIPT

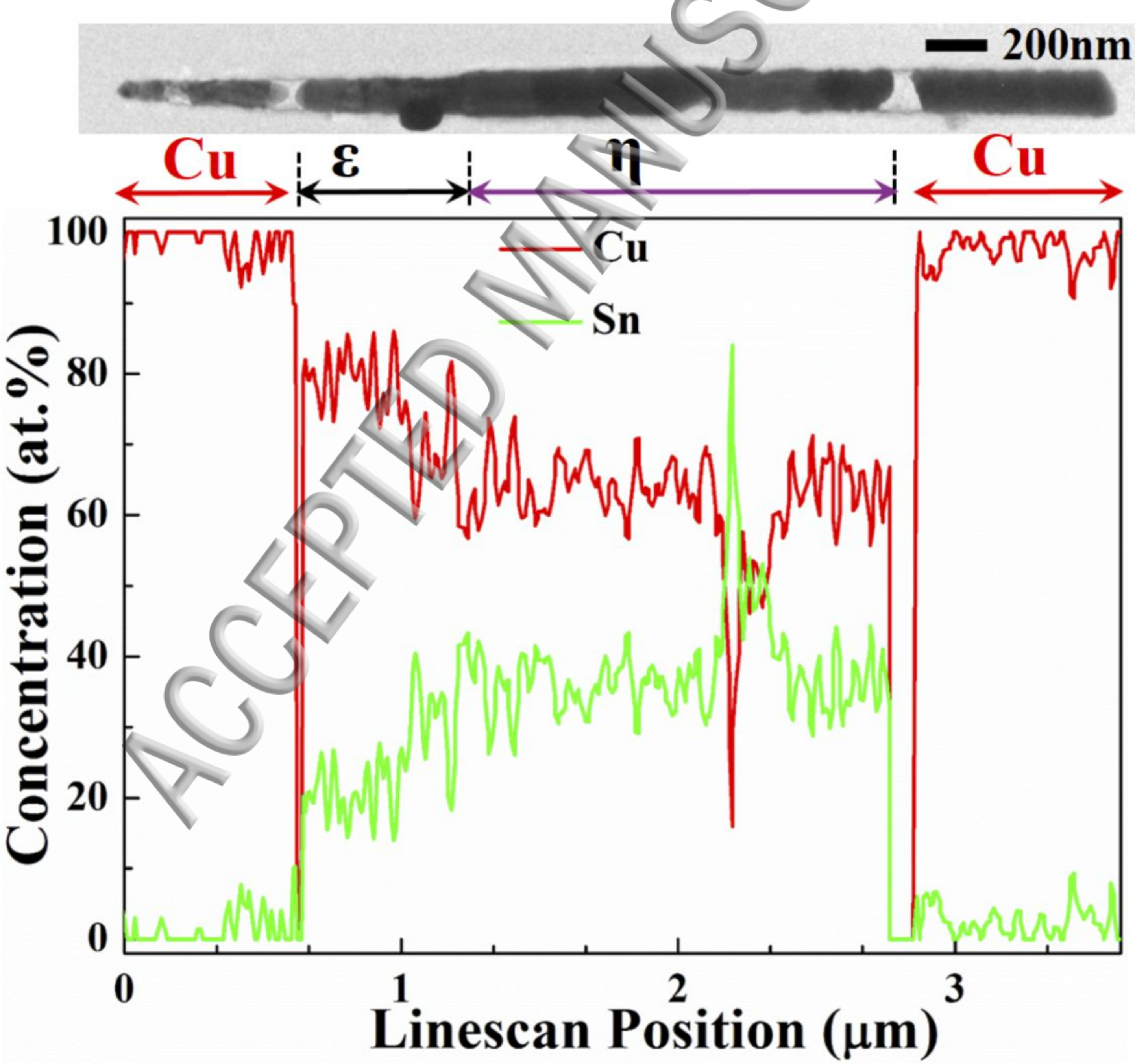

200nm
Cu
ε
η
Cu
100
80
60
40
20
0
Cu
Sn
Concentration (at.%)
0
1
2
3
Linescan Position (μm)

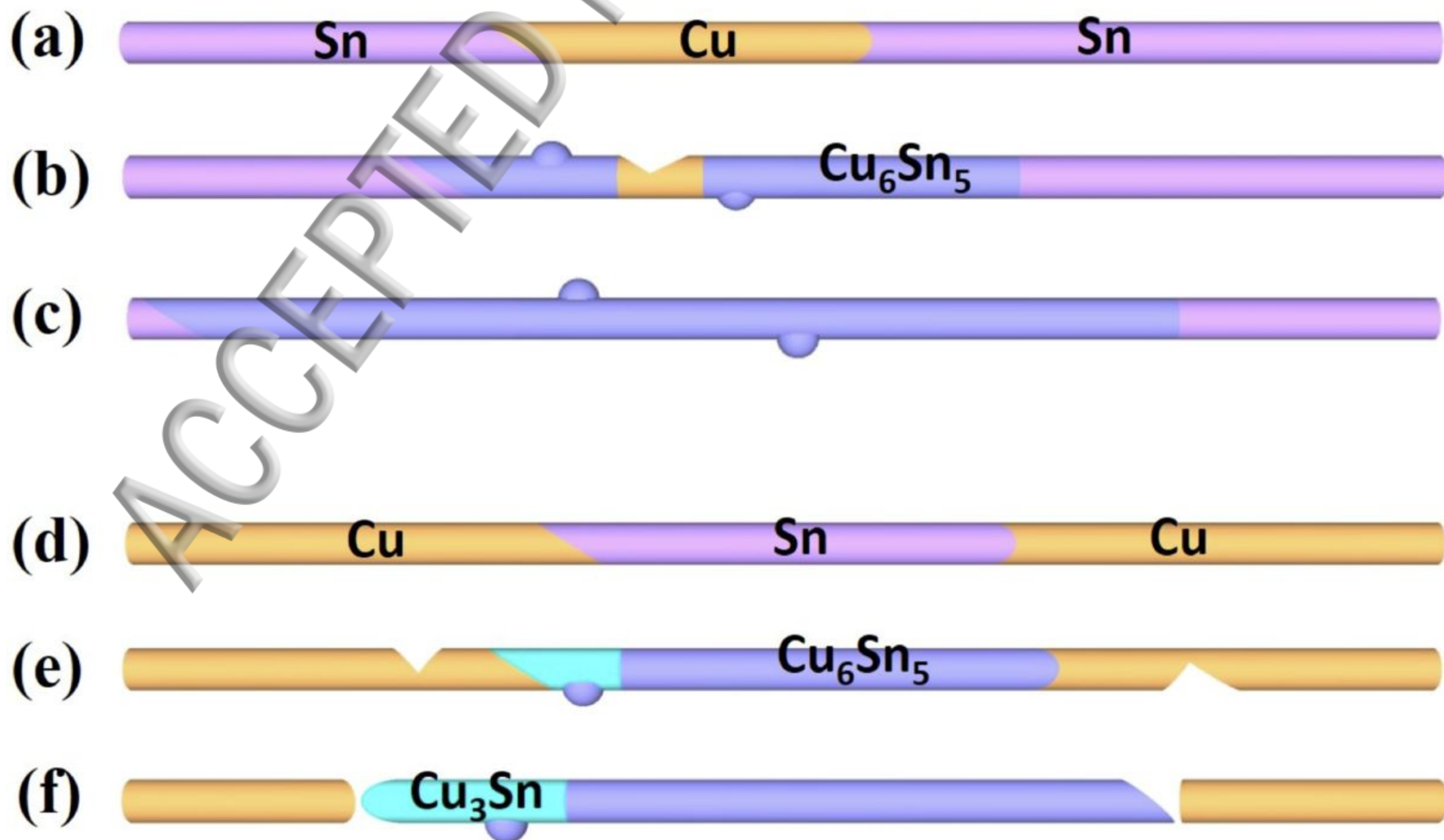

ACCEPTED M